A $\pm 45^{\circ}$-Polarized Antenna System for In-Band Full-Duplex (IBFD) with Four Isolated Channels

Yue-Nian Chen, *Student Member, IEEE*, Can Ding, *Member, IEEE*, He Zhu, *Member, IEEE*, and Ying Liu, *Senior Member, IEEE*

***Abstract*—An in-band full-duplex (IBFD) antenna system having four ports with good self-interference cancellation (SIC) is presented in this paper. Two of the four ports provide $+45^{\circ}$-polarized radiation and the other two generate -45°-polarized radiation. Every port of the proposed antenna is well isolated from the other three ports, enabling simultaneous transmitting and receiving with both two polarizations. To achieve this goal, three different types of couplings need to be addressed simultaneously. In this work, a novel isolation feed network is proposed, which is the first of its kind that can achieve three targets at the same time, i.e., feeding the antenna differentially, forming the original horizontal and vertical polarizations into $\pm 45^{\circ}$ polarizations, and cancelling out the reflected and coupled signals between the transmitting (TX) and receiving (RX) ports. Then, a double-antenna IBFD system with four isolated channels is attained by combining the proposed feed network, defected ground structure (DGS), cross-shaped walls, and metal baffles, which effectively mitigated all the three types of couplings at the same time. The double-antenna system has high isolations of $>$ 39 dB between any two of the four ports from 3.3 to 3.9 GHz. The four radiation patterns obtained by exciting the four ports are very similar to each other and are stable with frequency, which makes it an excellent candidate for 5G sub-6 GHz IBFD applications.**

***Index Terms*—Dual-polarization, four isolated ports, in-band full-duplex (IBFD), isolation feed network, self-interference cancellation (SIC).**

I. Introduction

As more and more wireless devices need to operate at different frequency bands to avoid interferences, spectrum has become a scarce and precious resource. In-band full-duplex (IBFD) has drawn great interests and attentions in both academics and industries [1]–[4], as it can theoretically double the spectrum efficiency compared with traditional half-duplex (HD) transmission techniques, i.e., time-division duplex (TDD) and frequency-division duplex (FDD). However, the realization of IBFD poses a great challenge, i.e., how to minimize the tremendous self-interference (SI) between the transmitting (TX) and receiving (RX) ports. Self-interference cancellation (SIC) techniques are promising solutions to reduce the SI and enable IBFD. They can be implemented in the digital-domain, analog-domain, and/or antenna-domain. Among them, reducing the SI in the antenna-domain is the first defense barrier and it has a much lower cost compared to those in the digital- and analog-domains. The SIC approaches in the antenna-domain are usually passive methods thus they are not as powerful as the active methods in the other domains. However, maximizing the performance of passive SIC can significantly alleviate the complexity and pressure of the next active SIC circuits or algorithms, which can greatly reduce the overall cost of the entire IBFD system [5]. Therefore, an antenna system with high isolation between the TX and RX ports are critical to the IBFD wireless communication. Besides the isolation, there are also several other critical factors for an antenna system to be suitable for IBFD application, e.g., size, bandwidth, radiation pattern, gain, etc.

A straightforward method to attain two isolated signal channels for IBFD is to employ two independent antennas, i.e., one for TX and the other for RX, and physically separate them as much as possible [6]. However, this traditional approach is not preferred as the performance is limited and the size can be quite large. To maintain a compact size of antenna, many SIC techniques have been reported and they can be generally classified into two categories, i.e., multiple-antenna and single/shared-antenna systems, depending on the number of antennas employed.

Similar to that of the traditional antenna separation, the SIC techniques utilizing multiple antennas have one or more antennas work as TX antennas and the others work as RX antennas. But these techniques are able to reduce the couplings between the TX and RX antennas despite the close proximity between them. Decoupling structure/network is a very popular kind of methods to effectively improve the isolation in multiple-antenna systems. It can suppress the coupling wave by introducing an additional coupling path with opposite phase to cancel out the original coupling, such as defected ground structure (DGS) [7], wave trap structure (WTS) [8], high impedance surface (HIS) [9], frequency selective surface (FSS) [10], antenna decoupling surface (ADS) [11], and neutralization line (NL) [12]. On the other hand, high isolation can be also acquired by elaborately locating the TX/RX antenna at the near-field null of the RX/TX antennas with specific phase excitations, which is known as near-field cancellation [13]–[15].

Compared to multiple-antenna IBFD systems, single/shared

This work was supported in part by the National Natural Science Foundation of China, grant number No. 61871309, No. 61801346 and also by the Australian Research Council (ARC) DECRA under grant DE200101347. (*Corresponding author: Can Ding*.)

Yue-Nian Chen is with National Key Laboratory of Antennas and Microwave Technology, Xidian University, Xi'an 710071, China. He is also with the Global Big Data Technologies Center, University of Technology Sydney, Ultimo, NSW 2007, Australia (e-mail: Chenynxxx@126.com).

Ying Liu is with National Key Laboratory of Antennas and Microwave Technology, Xidian University, Xi'an 710071, China (e-mail: liuying@mail.xidian.edu.cn).

Can Ding and He Zhu are with the Global Big Data Technologies Center, University of Technology Sydney, Ultimo, NSW 2007, Australia (e-mail: Can.Ding@uts.edu.au, He.Zhu@uts.edu.au).

antenna IBFD systems are more preferred in many modern communication platforms where different kinds of antennas are collocated in a constrained space to enable multifunction [16] . This is because the single/shared IBFD systems use less antenna elements, which saves space for antenna installation and alleviates unwanted couplings with other antennas. The most commonly seen implementation is various kinds of dual-polarized antennas which make use of the inherent high isolation between the two orthogonal polarizations [17]–[23]. The isolation between the two polarizations can be further enhanced by using differential feed, e.g., an extremely high isolation of 80 dB was achieved in [24] by exciting the TX mode through a single-fed patch while realizing the RX mode through another adjacent differential-fed patch. Besides the dual-polarized antennas, one could also excite two orthogonal modes on a single antenna, such as the two characteristic modes with 58 dB isolation in [25], the even and odd modes with 50 dB in [26], and the common and differential modes in [27], [28]. In [29], by exploring a shared aperture cavity-like structure with two highly orthogonal modes (quarter-wavelength slot mode and half-mode cavity mode), high isolation between the TX and RX ports was realized. These aforementioned single/shared antennas always use one polarization for TX and the other one for RX. In fact, a single-polarized antenna can also generate two isolated signal paths by utilizing circulators in its feed network [30]–[32]. However, the imperfection of the circulators usually leads to deteriorated performance in practice. There are also some works [33]–[35] using only hybrid couplers to cancel unwanted signals at RX port, realizing high isolation between the two single paths having the same polarization.

Since simultaneous transmission and receiving can be attained using one antenna with one polarization or two orthogonal polarizations, it occurred to us that one may generate four signal paths that are well isolated from each other (two channels for each polarization) and any two of them can be regarded as TX and the other two are for RX. This way, the spectrum efficiency can be maximized and the polarization diversity can combat the multi-path effect. To achieve this goal, three types of couplings need to be suppressed simultaneously, which are the cross-polarization coupling between the two ports of the same antenna, the co-polarization coupling between adjacent antennas, and the cross-polarization coupling between adjacent antennas. The three types of couplings are defined as type I, type II, and type III couplings, respectively. Compared to those two-channel IBFD systems that focus only on one type of coupling (type I or type II), this target is much more challenging. There are a few attempts published in the literatures, but their performance is limited [36]–[38]. For example, the bandwidth is only 6.45% in [37] and the worst isolation is only 27 dB and 17 dB in [36] and [38], respectively.

In this paper, a compact IBFD antenna system with four isolated channels is proposed for cellular base station application. Three types of couplings are addressed in a holistic way using a new multifunctional isolation feed network and some existing monostatic and bi-static cancellation approaches. We firstly designed a dual-polarized patch antenna, which is fed differentially to ensure a high degree of symmetry to facilitate the SIC. A novel isolation feed network is developed to differentially feed the antenna and to combine the original horizontal and vertical polarizations into $\pm 45^\circ$ polarizations for base station applications. More importantly, the isolation feed network is able to cancel out the signal couplings and reflections caused by imperfections, alleviating the type I coupling. It is the first single antenna IBFD system that achieves $\pm 45^\circ$ polarizations by combining the H/V polarizations rather than rotating the naturally square patches, which reduces the edge-to-edge distance between adjacent antennas when used in array and thus mitigates the type II and III couplings. Then, based on the proposed single antenna element, a 1×2 antenna array is constructed that has four isolated ports. Additional DGS, cross-shaped walls, and metal baffles are introduced to further reduce the type II and III couplings without deteriorating the type I coupling. The obtained double-antenna system enables simultaneous transmission and receiving in both the two polarizations across a wide bandwidth from 3.3 to 3.9 GHz (16.6%) with the isolations among any two ports are >39 dB. Both the single-antenna and the double-antenna systems are compared to the comparable state-of-the-art works to illustrate their superiority.

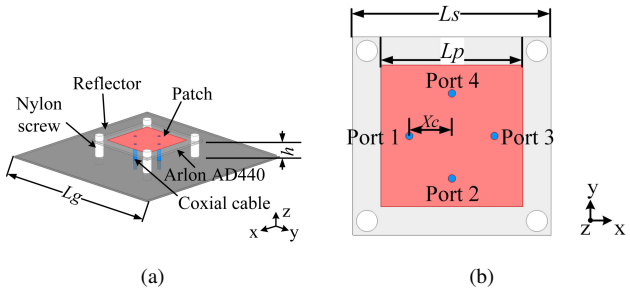

Fig. 1. Antenna configuration. (a) Perspective view. (b) Front view of the patch. (Dimensions : Lg = 100 mm, Ls = 42 mm, Lp = 30 mm, Xc = 9 mm)

II. Antenna Element

Fig. 1(a) gives the perspective view of the proposed antenna element, which consists of a square patch radiator, a reflector, and two pairs of coaxial cables for differential feeding. The square patch is printed on the top of the substrate Arlon AD440 with a dielectric constant of 4.4, a loss tangent of 0.005, and a thickness of 1 mm. The substrate is mounted above the reflector with the height of h = 8 mm to enhance the operation bandwidth of the patch antenna. Four nylon screws are used to support the substrate. The inner and outer conductors of the cables are connected to the patch and the reflector, respectively. The front view of the radiator is shown in Fig. 1(b). Two pairs of cables are connected to the patch and the distances between any feed port and the center of the square are identical, i.e., Xc = 9 mm.

Note that the antenna is designed to be fed differentially to provide good symmetry and to suppress the cross-polarization radiation, which assists with the decoupling but poses a challenge to the design of its feed network. By feeding ports 1 and 3 differentially, horizontal-polarized radiation can be

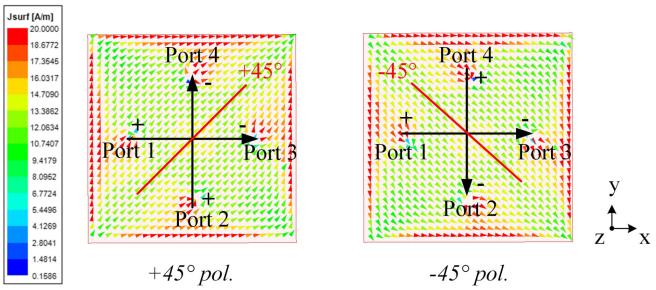

Fig. 2. The current distribution on the patch for the $+45°$° polarization and $-45°$ polarization.

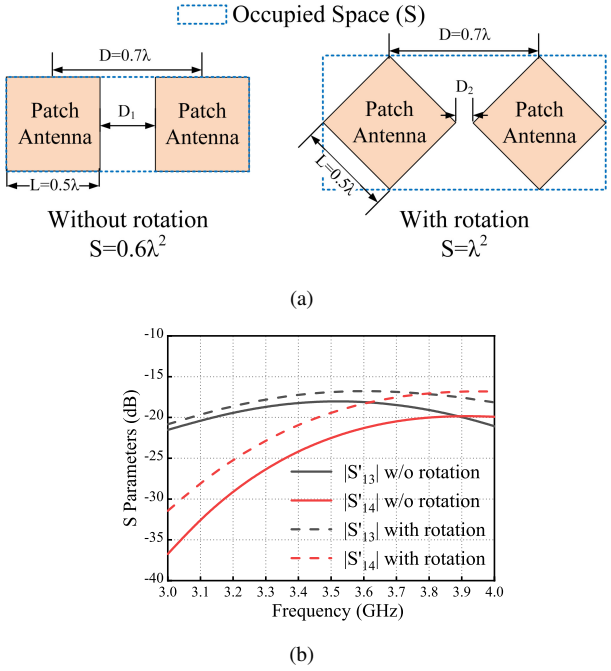

Fig. 3. (a) Geometry of two $\pm 45°$-polarized antenna arrays employing two square patch antennas without and with the $45°$ rotation. (b) The type II (S'_{13}) and III (S'_{14}) couplings between the adjacent patches for the two geometries.

attained; by feeding ports 2 and 4 differentially, vertical-polarized radiation can be obtained. As shown in Fig. 2, in this work, the two pairs of differential ports are excited simultaneously with the same or opposite phases to get $\pm 45°$ polarizations for base station applications.

It's worth to mention that the $\pm 45°$-polarization can also be attained by rotating a naturally H/V-polarized square patch. However, as shown in Fig. 3, the rotation of the elements can lead to larger size and stronger couplings between adjacent antennas (type II and III couplings) when used in arrays. It can be easily found in Fig. 3(a) that, with the same centre-to-centre distance, the antenna array without rotation occupied 40% less space compared to the rotated array. Meanwhile, the edge-to-edge spacing of the array without rotation is much larger than that of the rotated array, which leads to lower type II and III couplings as illustrated in Fig. 3(b).

The simulated reflection coefficients and realized gains of the proposed antenna element (with ideal feeding) are depicted in Fig. 4. The S'_{11} and S'_{22} represent the reflection coefficients

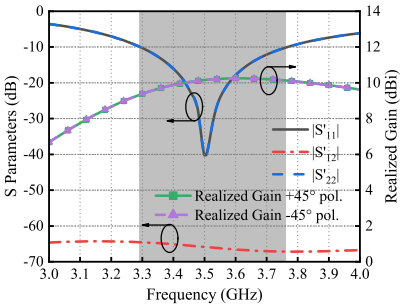

Fig. 4. Simulated reflection coefficients and realized gains of the dual-polarized antenna element.

of the $+45°$ polarization and $-45°$ polarization, respectively. Due to the symmetry, the reflection coefficients as well as the realized gains of the two polarizations are identical. S'_{12} is the transmission coefficient between the two polarizations. The coefficients were calculated in the following equations.

$$S'_{11} = (S_{dd11} + S_{dd12} + S_{dd21} + S_{dd22})/2 \quad (1)$$

$$S'_{22} = (S_{dd11} - S_{dd12} - S_{dd21} + S_{dd22})/2 \quad (2)$$

$$S'_{12} = (S_{dd11} - S_{dd12} + S_{dd21} - S_{dd22})/2 \quad (3)$$

where S_{dd} is the differential S parameter matrix in a dual-polarized differential antenna, which can be expressed as [39]:

$$S_{dd} = \begin{bmatrix} S_{11} - S_{31} - S_{13} + S_{33} & S_{12} - S_{32} - S_{14} + S_{34} \\ S_{21} - S_{41} - S_{23} + S_{43} & S_{22} - S_{42} - S_{24} + S_{44} \end{bmatrix} \quad (4)$$

As shown in Fig. 4, both the $\pm 45°$ polarizations cover a bandwidth of 3.29 – 3.76 GHz with a realized gain around 10 dBi and the isolation between them is $>$ 65 dB. Although theoretically the isolation between the two polarizations of the patch antenna is very high, a feed network is required to excite the antenna in a proper way, which will inevitably deteriorate the isolation.

III. Isolation Feed Network

A. Configuration and working mechanism

Fig. 5 shows the configuration of the isolation feed network and illustrates how the feed network is connected to the antenna and excites the $\pm 45°$ polarizations. The network consists of four identical $180°$ hybrid couplers and has four input and four output ports. The four output ports (P1 to P4) are connected to the four coaxial cables of the patch antenna. As shown in the figure, only two of the input ports are used while the other two are loaded with 50 Ω resistances. Bear in mind that an input signal at the sum (Σ) or differential inputs (Δ) of the hybrid coupler leads to in-phase or out-of-phase outputs, respectively, with equal amplitudes. By exciting any of the two input ports of the feed network, the input signal is split into the four outputs evenly but with different phase relationships. For example, when the TX port is excited (the signal path is labelled by red solid arrows), the phases at ports 1 to 4 are $0°$, $0°$, $180°$, and $180°$, respectively, leading to a $+45°$-polarized radiation. Similarly, when the RX port is excited (the signal path is labelled by blue solid arrows), the

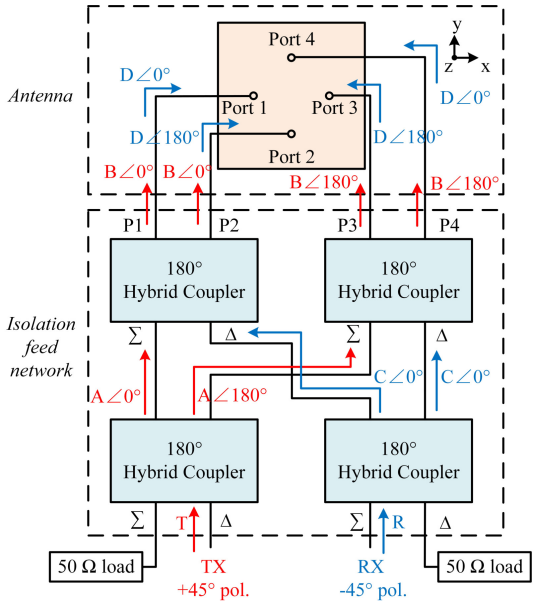

Fig. 5. Configuration of the isolation feed network and illustration of the signal paths.

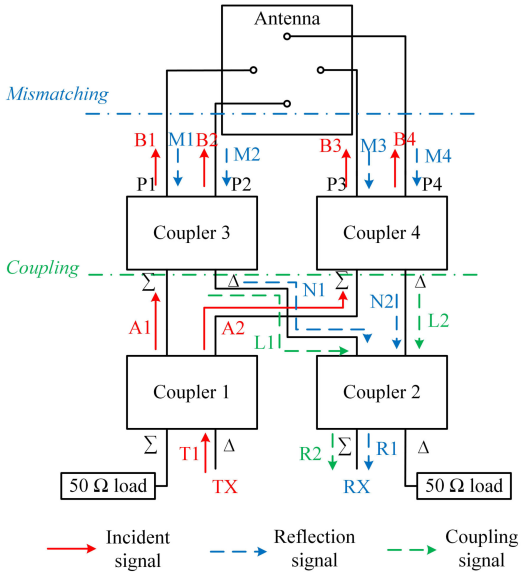

Fig. 6. Diagram of the signal flow in the single-antenna system.

phases at ports 1 to 4 are 0°, 180°, 180°, and 0°, respectively, exciting a $-45°$-polarized radiation.

More importantly, the proposed isolation feed network also has an ability to reduce the coupling between the TX and RX ports and its working mechanism is illustrated in Fig. 6. The red solid arrows represent the incident signal from the TX port. Ideally, the TX signal will all flow into the antenna and then radiate, thus there will be no signal going back to the RX port so that the isolation between the TX and RX ports is infinite. However, in reality, the antenna mismatching and the coupling between the sum and differential ports of the couplers could significantly decline the performance. In this work, the proposed isolation feed network is capable of self-cancelling the couplings caused by these imperfections.

The first imperfection that causes self-interference is the impedance mismatching between the feed network and the antenna, which will introduce extra reflection signals flowing into the RX port. The signal flow of the reflection is highlighted using blue dash arrows in Fig. 6. As shown in the figure, due to mismatching, there will be four signals ($M1$ – $M4$) reflected from the antenna port and going back into the second-stage hybrid couplers, i.e., Couplers 3 and 4. Since the configuration is symmetric, it is assumed that the four ports have the same reflection ratio. The reflected signals $M1$ – $M4$ can be calculated using

$$M1 = \alpha B1, M2 = \alpha B2, M3 = \alpha B3, M4 = \alpha B4 \quad (5)$$

where α is the reflection ratio between the antenna's input ports and the network's output ports. After passing through the second-stage couplers, $M1$ – $M4$ combined at the differential ports of Couplers 3 and 4 and turned into $N1$ and $N2$, where

$$\begin{aligned} N1 &= M1e^{j180^\circ} + M2 = M2 - M1 = \alpha(B2 - B1) \\ N2 &= M3e^{j180^\circ} + M4 = M4 - M3 = \alpha(B4 - B3) \end{aligned} \quad (6)$$

By comparing Fig. 5 and Fig. 6, it can be found that $B2 = B1$, $B3 = B4 = B1e^{j180^\circ}$. Therefore, $N1$ and $N2$ are both 0. Thus it can be concluded that the reflection signals are cancelled out after passing through the second-stage couplers. Note $M1$ – $M4$ also combine at the sum ports of Couplers 3 and 4, but the resultant signals will not enter the RX port, thus having no effect to the isolation between the TX and RX ports.

The second imperfection considered here is the coupling between the sum and differential ports of the two second-stage couplers, which are illustrated as green dash arrows $L1$ and $L2$. The same couplings of the two first-stage couplers will not affect the isolation between the TX and RX ports, thus they are not discussed here. The coupling signals $L1$ and $L2$ can be obtained as

$$L1 = \beta A1, L2 = \beta A2 \quad (7)$$

where β represents the coupling coefficient between the sum and differential ports of the couplers, and $A1$ and $A2$ are the output signals of the differential input port as shown in Fig. 6. Note $A1$ and $A2$ have the same amplitude and are out-of-phase:

$$A1 = A2e^{j180^\circ} = -A2 \quad (8)$$

The coupling signals $L1$ and $L2$ need to pass through Coupler 2 to enter the RX port. The signal received at the RX port can be calculated as

$$R2 = L1 + L2 = \beta A1 + \beta A2 = 0 \quad (9)$$

This indicates that the interferences caused by the couplers can also be neutralized by this isolation feed network.

We remark that this feed network is the first one that can hit three birds with one stone, i.e., providing differential feeding for an antenna with four ports, combining the initial horizontal and vertical polarizations into $\pm 45°$ polarizations, and cancelling out signal reflection and coupling.

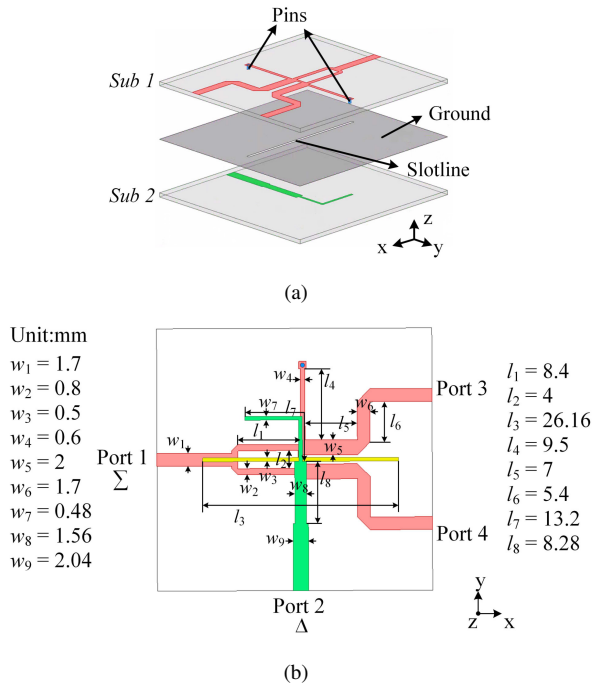

Fig. 7. Configuration of the 180° hybrid coupler. (a) Disassembled view. (b) Layout view.

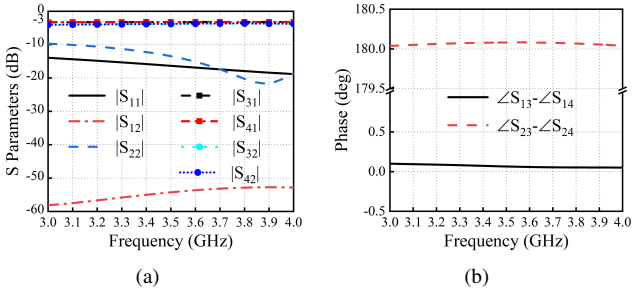

Fig. 8. Simulated results of the proposed coupler. (a) S parameters. (b) Phase differences at the outputs.

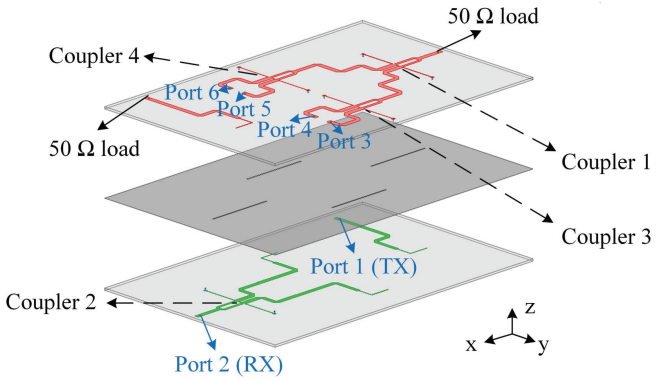

Fig. 9. Dissembled view of proposed feed network with four couplers.

B. Hybrid coupler

Although the proposed isolation feed network can eliminate the negative effect introduced by the couplings between the sum and differential ports of the couplers, it exaggerates the performance degradation resulted from the amplitude and phase errors between the couplers' output ports. Therefore, the performance of the couplers, especially the amplitude and phase errors, is critical to system performance. The 180° hybrid couplers used in this work were designed based on microstrip-to-slotline transformer and slotline resonator following the principle described in [40], [41]. As shown in Fig. 7(a), the coupler consists of two substrates, i.e., Sub 1 and Sub 2, both of which have the dielectric constant of 4.4 and the height of 0.762 mm. The sum mode transmission lines (highlighted in red) and the differential mode transmission lines (highlighted in green) are printed on the top layer of Sub1 and on the bottom layer of Sub 2, respectively. Between Sub 1 and Sub 2 is the ground layer with a slotline that is used to offer differential signals. The detailed dimensions are given in Fig. 7(b). Note that port 1 is the sum port, port 2 is the differential port, and ports 3 and 4 are the output ports. The simulated S parameters of the coupler are given in Fig. 8. As shown in Fig. 8(a), the coupler covers a wide bandwidth of 3 – 4 GHz with the reflection coefficients <-10 dB. The isolation between the sum and differential ports is >52 dB thanks to the slotline that separates the sum and differential signals [40]. The transmission coefficients from port 1 to the output ports and from port 2 to the output ports are 3.3 dB and 3.8 dB at 3.5 GHz, respectively and they are stable within the bandwidth. The maximum insertion loss is less than 0.9 dB. As revealed in Fig. 8(b), the phase differences at the two outputs when feeding from ports 1 and 2 are about 0° and 180° with extremely small errors.

C. Prototype and measurement

Fig. 9 presents the layout of the isolation feed network constructed by the couplers designed in the previous subsection. Similar to the couplers, the isolation feed network has two substrate layers and three metal layers. The four couplers are connected quasi-symmetrically to minimize the amplitude and phase errors that might deteriorate the system performance. In specific, Couplers 3 and 4 are placed symmetric with respect to the y-axis, while Couplers 1 and 2 are symmetric with respect to the x-axis. This is to ensure the lengths of connection lines between the first-stage and second-stage couplers are uniform, thus avoiding extra amplitude and phase errors. The port 1 and port 2 located on the bottom layer are the two isolated input ports and they are denoted as the TX and RX ports, respectively. Ports 3 to 6 on the top layer are the four output ports that will be connected to the antenna. Another two input ports on the top layer are loaded with 50 Ω resistance. The size of the network is 115.8 mm × 76.42 mm.

The network was also fabricated and tested in the VNA with the dynamic range of more than 130 dB. The picture of the prototype is given in Fig. 10. The simulated and measured results of the proposed isolation feed network are presented in Fig. 11. It can be seen from Fig. 11(a) that the network can cover the bandwidth from 3.17 to 4 GHz with a high isolation of more than 51 dB between the TX and RX ports. As depicted in Fig. 11(b) and 11(c), the measured transmission parameters form TX port (port 1) and RX port (port 2) to the

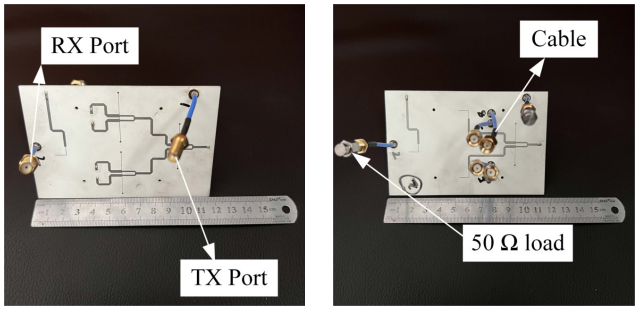

(a) (b)

Fig. 10. Prototype of proposed isolation feed network. (a) Top view. (b) Bottom view.

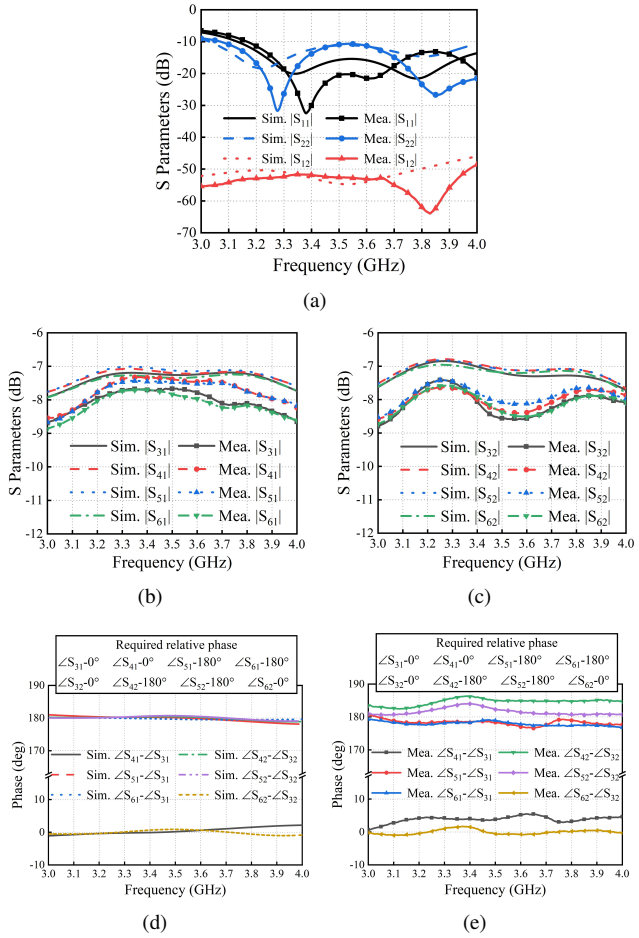

(a) (b) (c) (d) (e)

Fig. 11. Simulated and measured results of the proposed isolation feed network. (a) The reflection coefficients of and the isolation between the TX and RX ports. (b) The transmission coefficients from the TX port to the output ports. (c) The transmission coefficients from the RX port to the output ports. (d) Simulated phase difference between the output ports when the TX or RX port is excited. (e) Measured phase difference between the output ports when the TX or RX port is excited.

output ports are 7.95±0.65 dB and 8±0.6 dB, which are close to the simulated results of 7.4 ±0.4 dB and 7.25±0.5 dB. It is observed that there is a discrepancy of around 1 dB between the simulated and measured transmission coefficients. This is mainly due to the extra losses of the SMA connectors and coaxial cables. The simulated and measured phase differences between the output ports are shown in Fig. 11(d) and 11(e),

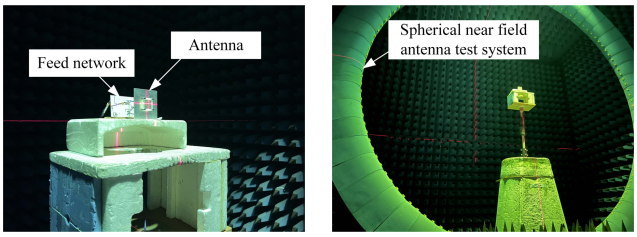

(a) (b)

Fig. 12. Photo of the single-antenna system under test. (a) Perspective view of the antenna system. (b) Test environment.

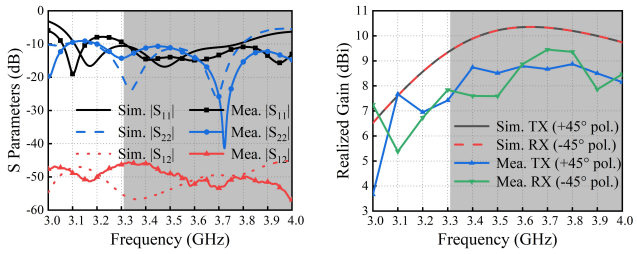

(a) (b)

Fig. 13. Simulated and measured results of proposed IBFD single antenna system. (a) S parameters. (b) Realized gains.

which reveals that the phase errors are less than 5°. These errors are attributed to the superimposed phase errors of single couplers (1° – 1.5°) and the different length of the cables (3° – 4°). Note that the cables used in the experiment were simply cut with a scissor for cost purpose. We remark that by cutting the cables with a professional machine to ensure the uniformity can significantly reduce the phase error and improve the performance of the entire system.

IV. Single-Antenna System with Two Isolated Channels for IBFD

The feed network was then connected with the antenna element to form into a single-antenna system for IBFD applications. The prototype of the antenna system and the test setup are shown in Fig. 12. The simulated and measured S parameters and realized gains of the single-antenna system are depicted in Fig. 13(a) and 13(b), respectively. The measured and simulated S parameters agree well with each other in general. The measured impedance bandwidth is 3.31 – 4 GHz, which is slightly shifted to the high frequency compared to the simulated bandwidth of 3.18 – 3.78 GHz. It is mainly due to the dielectric constant error of the substrates and the imperfect compression of the multi-layers. The measured $|S_{12}|$ is also shifted to the higher frequency but the worst isolation is similar to the simulated one, i.e., 46 dB. As shown in Fig. 13(b), the measured gains vary from 7.5 to 8.9 dBi and from 7.9 to 9.4 dBi for the $+45°$ and $-45°$ polarizations, respectively, across the measured bandwidth. The measured gains are lower than the simulated ones by virtue of the extra insertion losses of the cables and SMA connectors.

The simulated and measured radiation patterns in the *xoz* and *yoz* planes of the two polarizations at 3.3 GHz, 3.6 GHz, and 3.9 GHz are given in Fig. 14. Good agreements between

TABLE I
COMPARISON WITH IBFD ANTENNAS WITH INTEGRATED ISOLATION FEED NETWORK

Ref.	SIC Methods	The Num. of Ant.	Polarizations	Size (λ_0^2)	Bandwidth	Gain (dBi)	Isolation (dB)
[31]	IFN	2	TX: RHCP RX: RHCP	1.7 × 1.7	0.5 - 3.5 GHz (150%)	> -5	> 37
[32]	IFN	1	TX: RHCP RX: RHCP	2π × 16 (Reflector)	4 - 8 GHz (66.7%)	> 21	> 30
[33]	IFN	1	TX: RHCP RX: RHCP	2π × 16 (Reflector)	4 - 8 GHz (66.67%)	RX: > 7 TX: > 20	61 (average)
[34]	IFN	4	TX: RHCP RX: RHCP	1.6 × 1.6	2.4 - 2.5 GHz (16.22%)	> 7	> 47
[35]	IFN	4	TX: V-pol. RX: V-pol.	NG	1.75 - 1.85 GHz (14%)	-	> 30
Proposed Ant.1	**DF,PO,IFN**	**1**	**TX: $+45°$-pol.** **RX: $-45°$-pol.**	**1.2 × 1.2**	**3.31 - 4 GHz (18.5%)**	**> 7.5** **Max: 9.45**	**> 46**

IFN: isolation feed network; DF: differential feed; PO: polarization orthogonality;
NG: not given.

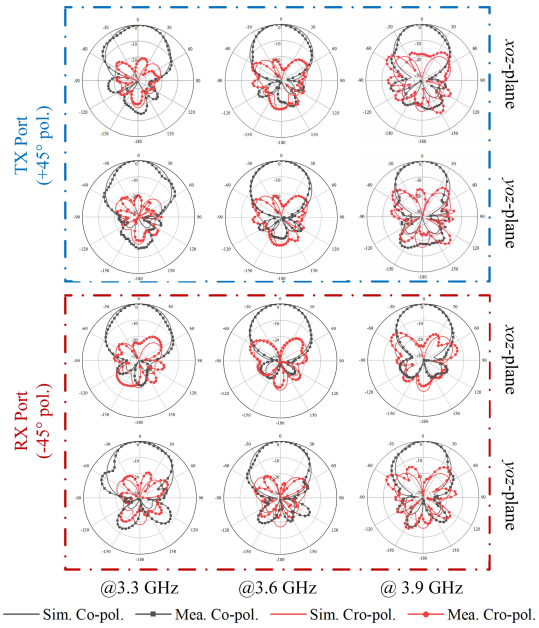

Fig. 14. Simulated and measured radiation patterns of the proposed single antenna system for its two polarizations.

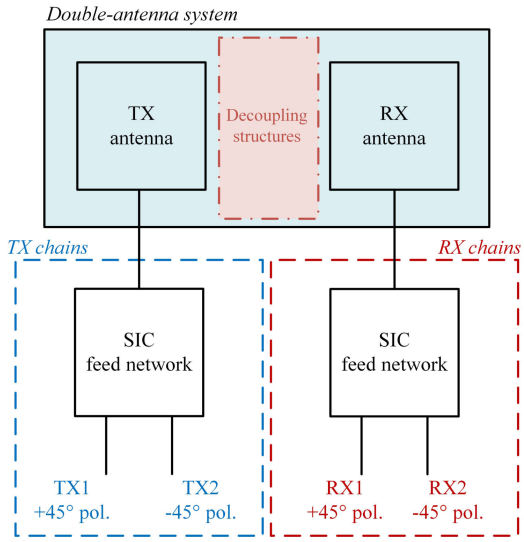

Fig. 15. The mechanism diagram of proposed double-antenna system for IBFD.

the simulated and the measured radiation patterns are achieved and the patterns of the TX and RX modes are similar and stable within the operation bandwidth. The measured half-power beam widths (HPBWs) are 41° – 53° and 42° – 54° from 3.3 GHz to 4 GHz for the TX and RX modes, respectively.

Note that high isolation can be obtained between the two polarizations of a dual-polarized antenna by exciting the two polarizations with two feed networks that are physically separated apart. However, designing an integrated feed network to excite two polarizations simultaneously is more preferable (also more challenging). Table I compares the attained antenna system with the state-of-the-art IBFD antennas based on integrated isolation feed networks. It can be revealed from the table that while the performance of this single-antenna system is comparable to the others, it is the only one that generates $\pm 45°$ polarizations for base station applications.

V. DOUBLE-ANTENNA SYSTEM WITH FOUR ISOLATED CHANNELS FOR IBFD

As shown in Fig. 15, by placing two single-antenna systems side-by-side, a double-antenna system with four ports is obtained. The target is to maintain low couplings between any two of the four ports so that simultaneous transmission and receiving with both the two polarizations can be realized. Preferably, one antenna is used for TX and the other is used for RX and both the two antennas are dual-polarized.

As revealed in the last section, the couplings between the two ports of a same antenna can be kept low thanks to the proposed isolation feed network. The challenge here is to enhance the isolation between the same polarizations of the TX and RX antennas, e.g., between TX1 and RX1. Fig. 16 illustrates the evolvement of the antenna configuration to mitigate the couplings between the adjacent antennas. As shown in Fig. 16, Conf. 1 is the conventional coupled array with the central spacing S = 100 mm (1.17 λ at 3.5 GHz). In Conf. 2, metal baffles surrounding the elements are introduced to form isolated cavities, which reduces the space coupling.

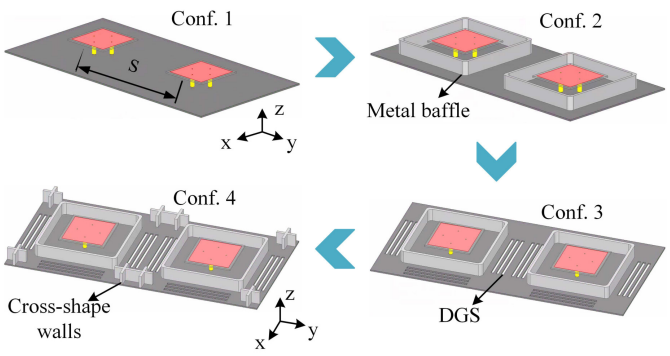

Fig. 16. Configuration evolvement of the double-antenna system.

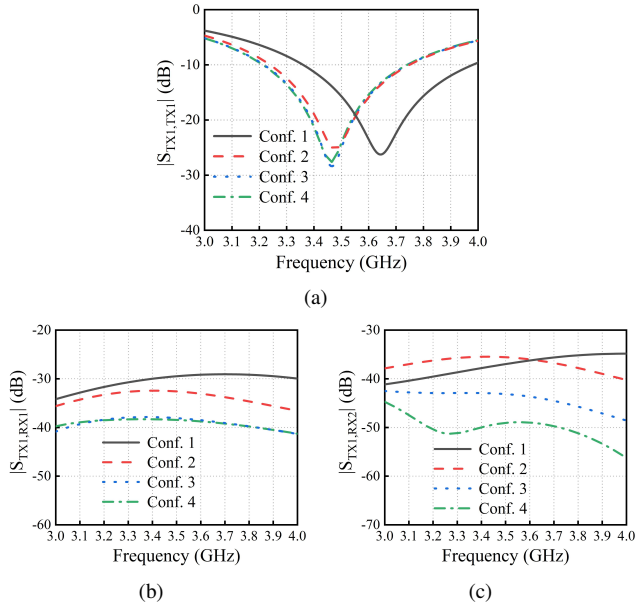

Fig. 17. Simulated S parameters of the four configurations without isolation feed networks. (a) Reflection coefficient of port TX1. (b) Transmission coefficient between the ports having the same polarization. (c) Transmission coefficient between the ports having different polarizations.

The size of each cavity is 65 mm × 65 mm × 10 mm. Then a defected grounded structure (DGS) is employed in Conf. 3 to suppress the surface coupling on the ground. The DGS has six slots, and the size of each slot is 50 mm × 2 mm. In the final configuration, cross-shape metal walls are utilized to eliminate the cross-polarization currents, leading to a significant enhancement of the isolation between the two different polarizations (between TX1 and RX2 and between TX2 and RX1).

The variation of the S parameters during the antenna evolvement are depicted in Fig. 17. It should be noted that all the results are obtained with an ideal feed network and the S parameters are calculated using equations (1) – (4). As shown in Fig. 17(a), adding the decoupling structures does not change the working bandwidth of the element except that the operation band shifts to the lower frequency after introducing the metal baffles. Meanwhile, Fig. 17(b) and 17(c) intuitively demonstrates how the isolation is gradually improved by adding these easy-to-implement and low-cost

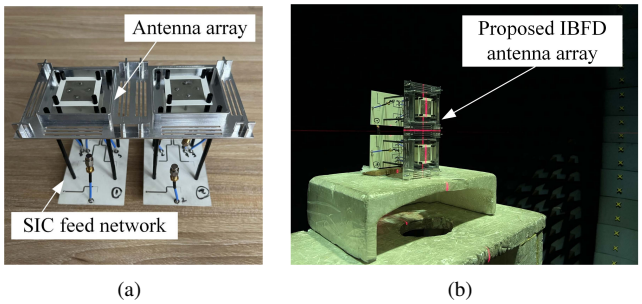

Fig. 18. Photograph of (a) fabricated prototype. (b) test environment.

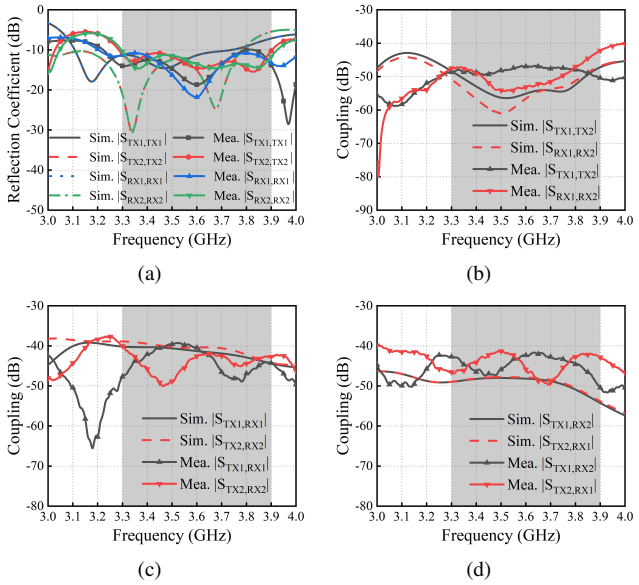

Fig. 19. Simulated and measured S parameters of proposed double-antenna system. (a) Reflection coefficients. (b) Transmission coefficients between the two ports of the same antenna. (c) Transmission coefficients between the ports having the same polarizations. (d) Transmission coefficients between the ports having different polarizations.

decoupling structures. It can be seen that the coupling between the ports having the same polarization is improved from 29 dB to 38 dB, while the one between the ports having different polarizations is also enhanced from 35 dB to 49 dB within the operation bandwidth.

The double-antenna system was also fabricated, assembled, and tested. The photos of the prototype and the test setup are given in Fig. 18. The simulated and measured S parameters of the proposed double-antenna system are plotted in Fig. 19. In general, the measured results agree well with the simulated ones. Some discrepancies are due to the loss introduced by the cables and SMA connectors, and they are unavoidable considering the signal levels are very low. As seen from Fig. 19(a), the measured -10 dB impedance bandwidth for all the four ports are from 3.3 GHz to 3.9 GHz, which is improved compared with the antenna array without the feed network. Fig. 19(b) demonstrates the cross-polarization couplings between the two ports of the each dual-polarized antenna, which are below -43 dB. As shown in Fig. 19(c), the measured same-polarization isolations between the TX and RX antennas are >39 dB. It is noted that the simulated

TABLE II
COMPARISON WITH IBFD ANTENNAS WITH FOUR CHANNELS

Ref.	SIC Methods	The Num. of Ant.	Polarizations	Bandwidth	Gain (dBi/dBic)	XPD (dB)	Isolation (dB)	Uniform Radiation Patterns When Exciting Different Ports
[36]	PO,IFN	1	TX: two CPs RX: two CPs	2 – 8 GHz (120%)	>3	NG	>27	No
[37]	PO,IFN	TX: 2 RX: 2	TX: two CPs RX: two CPs	6.0 – 6.4 GHz (6.45%)	>7.8	>10	>38	Yes
[38]	IFN, NFC	TX: 4 RX: 1	TX: two CPs RX: two CPs	0.8 – 3 GHz (116%)	TX: >4 RX: >-5	>5	>17	No
Proposed Ant. 2	**PO, IFN, DS**	**TX: 1 RX: 1**	**TX: $\pm45°$ pols RX: $\pm45°$ pols**	**3.3 – 3.9 GHz (16.6%)**	**>6.2**	**>18**	**>39.2**	**Yes**

PO: polarization orthogonality; IFN: isolation feed network; NFC: near-field cancellation; DS: decoupling structure;
XPD: cross-polarization discrimination = co-pol radiation/cross-pol radiation; NG: not given.

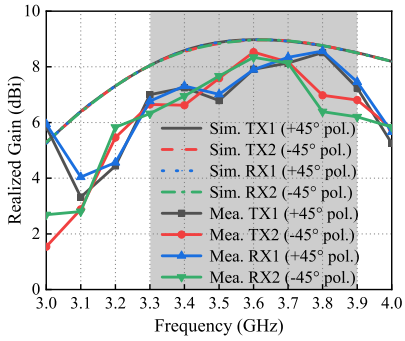

Fig. 20. Simulated and measured realized gains of the double-antenna system.

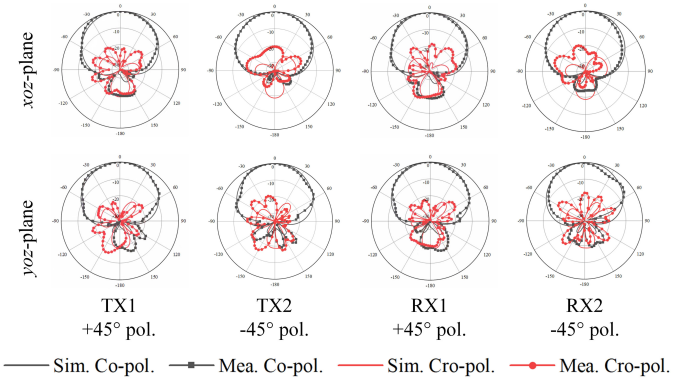

Fig. 21. Simulated and measured radiation patterns of the double-antenna system in the *xoz* and *yoz* plane at 3.5GHz.

isolation between TX1 and RX1 ports is >40 dB, which is about 2 dB larger than the array without the feed networks, indicating the proposed isolation feed network is also able to slightly improve the same-polarization isolation. Meanwhile, the isolations between the ports of the two antennas having different polarizations are >42 dB. To sum up, the isolation between any two ports of the double-antenna system for IBFD are >39 dB within the bandwidth of 3.3 – 3.9 GHz.

Fig. 20 shows the simulated and measured realized gains of all the four ports, which are more than 6.2 dBi and the maximum gain within the operation bandwidth is 8.6 dBi. It is noticed that the measured gain is lower than the simulated

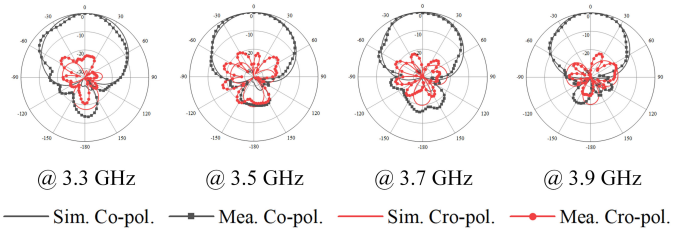

Fig. 22. Simulated and measured radiation patterns of the double-antenna system in the *xoz* plane of port TX1 at 3.3, 3.5, 3.7 and 3.9 GHz.

ones, which is mainly due to the extra insertion loss caused by the network, the cables, and the SMA connectors. By selecting cables and SMA connectors having better quality could improve the gain substantially.

The simulated and measured radiation patterns of all the ports at 3.5 GHz are given in Fig. 21. All the patterns are in nice shape and they are quite similar by exciting different ports. Fig. 22 plots the radiation patterns at different frequencies when exciting TX1 as an example. It can be concluded that the radiation patterns have a good consistency with the variation of frequency.

The proposed double-antenna system provides four isolated channels for IBFD application. It is able to simultaneously transmit and receive and both the transmission and receiving have two orthogonal polarizations. This leads to a higher diversity gain or a higher spectrum efficiency compared to the most available IBFD antennas having two isolated channels.

There are only a couple of papers that aimed at a similar goal as this work and a comparison is made in Table II. Compared to all these published IBFD antenna systems with four isolated ports, this work achieved the best isolation, which is significantly higher than [36] and [38] and is comparable to [37]. Although [37] has a decent isolation level, it used more elements and the bandwidth is quite narrow. Besides, thanks to the differential feeding, the proposed antenna has much lower cross-polarization radiation, i.e., the cross-polarization discrimination (XPD) within $-60°<\theta<60°$ is >18 dB. This paper is the only $\pm45°$-polarized design among the four comparable works, which is more challenging to obtain but is more demanded by base station applications. Additionally,

the radiation patterns attained by exciting all the four ports demonstrate very good uniformity and stability with frequency, which makes it an excellent potential IBFD solution for 5G sub-6 GHz base station applications.

VI. Conclusion

In this paper, an antenna system with four isolated ports enabling simultaneous transmission and receiving in both $\pm 45^{\circ}$-polarizations was developed. A differentially-fed patch antenna was selected as the antenna element. A new isolation feed network was proposed to feed the antenna and to improve the isolation between the two polarizations. It is capable of cancelling out the coupled and reflected signals caused by antenna mismatching and coupler deformation, leading to a high isolation between the TX and RX ports. By connecting the proposed feed network with the patch antenna, a single-antenna system was obtained with the isolation $>$ 46 dB within 18.5% bandwidth. Then, two single-antenna systems were placed side-by-side and decoupled to form into a double-antenna system that having the isolation between any two ports is $>$ 39 dB within 16.6% bandwidth. Both the single and double-antenna systems were fabricated, tested and compared to the comparable works to demonstrate their superiority.

References

[1] A. Sabharwal, P. Schniter, D. Guo, D. W. Bliss, S. Rangarajan, and R. Wichman, "In-band full-duplex wireless: Challenges and opportunities," *IEEE J. Sel. Areas Commun.*, vol. 32, no. 9, pp. 1637–1652, Sep. 2014.

[2] Z. Zhang, X. Chai, K. Long, A. V. Vasilakos, and L. Hanzo, "Full duplex techniques for 5G networks: Self-interference cancellation, protocol design, and relay selection," *IEEE Commun. Mag.*, vol. 53, no. 5, pp. 128–137, May 2015.

[3] G. Liu, F. R. Yu, H. Ji, V. C. M. Leung, and X. Li, "In-band full-duplex relaying: A survey, research issues and challenges," *IEEE Commun. Surveys Tuts.*, vol. 17, no. 2, pp. 500–524, 2nd Quart., 2015.

[4] D. Kim, H. Lee, and D. Hong, "A survey of in-band full-duplex transmission: From the perspective of PHY and MAC layers," *IEEE Commun. Surveys Tuts.*, vol. 17, no. 4, pp. 2017–2046, 4th Quart., 2015.

[5] Y. Chen, C. Ding, Y. Jia, and Y. Liu, "Antenna/propagation domain self-interference cancellation (SIC) for in-band full-duplex wireless communication systems," *Sensors*, vol. 22, no. 5, pp. 1699, Feb. 2022.

[6] E. Everett, A. Sahai, and A. Sabharwal, "Passive self-interference suppression for full-duplex infrastructure nodes," *IEEE Trans. Wireless Commun.*, vol. 13, no. 2, pp. 680–694, Jan. 2014.

[7] A. H. Hussein, H. H. Abdullah, M. A. Attia and A. M. Abada, "S-band compact microstrip full-duplex Tx/Rx patch antenna with high isolation," *IEEE Antennas Wireless Propag. Lett.*, vol. 18, no. 10, pp. 2090-2094, Oct. 2019.

[8] M. Heino, S. N. Venkatasubramanian, C. Icheln and K. Haneda, "Design of wavetraps for isolation improvement in compact in-band full-duplex relay antennas," *IEEE Trans. Antennas Propag.*, vol. 64, no. 3, pp. 1061-1070, Mar. 2016.

[9] P. V. Prasannakumar, M. A. Elmansouri and D. S. Filipovic, "Wideband decoupling techniques for dual-polarized bi-static simultaneous transmit and receive antenna subsystem," *IEEE Trans. Antennas Propag.*, vol. 65, no. 10, pp. 4991-5001, Oct. 2017.

[10] Y. Zhu, Y. Chen and S. Yang, "Decoupling and low-profile design of dual-band dual-polarized base station antennas using frequency-selective surface," *IEEE Trans. Antennas Propag.*, vol. 67, no. 8, pp. 5272-5281, Aug. 2019.

[11] K. Wu, C. Wei, X. Mei and Z. Zhang, "Array-antenna decoupling surface," *IEEE Trans. Antennas Propag.*, vol. 65, no. 12, pp. 6728-6738, Dec. 2017.

[12] S. Zhang and G. F. Pedersen, "Mutual coupling reduction for UWB MIMO antennas with a wideband neutralization line," *IEEE Antennas Wireless Propag.* Lett., vol. 15, pp. 166-169, 2016.

[13] L. Sun, Y. Li, Z. Zhang, and Z. Feng, "Compact co-horizontally polarized full-duplex antenna with omnidirectional patterns," *IEEE Antennas Wireless Propag.* Lett., vol. 18, no. 6, pp. 1154–1158, Jun. 2019.

[14] R. Lian, T. Y. Yin, Y. Yin, and N. Behdad, "A high-isolation, ultrawideband simultaneous transmit and receive antenna with monopole-like radiation characteristics," *IEEE Trans. Antennas Propag.*, vol. 66, no. 2, pp. 1002–1007, Feb. 2018.

[15] K. Kolodziej and B. Perry, "Vehicle-mounted STAR antenna isolation performance," in *Proc. IEEE Int. Symp. Antennas Propag.*, Jul. 2015, pp. 1602–1603.

[16] H. -H. Sun, C. Ding, H. Zhu, B. Jones and Y. J. Guo, "Suppression of cross-band scattering in multiband antenna arrays," *IEEE Trans. Antennas Propag.*, vol. 67, no. 4, pp. 2379-2389, April 2019.

[17] R. S. Hao, Y. J. Cheng, Y. F. Wu and Y. Fan, "A w-band low-profile dual-polarized reflectarray with integrated feed for in-band full-duplex application," *IEEE Trans. Antennas Propag.*, vol. 69, no. 11, pp. 7222-7230, Nov. 2021.

[18] Y. Zhang, S. Zhang, J. Li, and G. F. Pedersen, "A dual-polarized linear antenna array with improved isolation using a slotline-based 180° hybrid for full-duplex applications," *IEEE Antennas Wireless Propag. Lett.*, vol. 18, no. 2, pp. 348–352, Feb. 2019.

[19] Y.-M. Zhang and J.-L. Li, "A Differential-series-fed dual-polarized traveling-wave array for full-duplex applications," *IEEE Trans. Antennas Propag.*, vol. 68, no. 5, pp. 4097-4102, May 2020.

[20] D. Wójcik, M. Surma, A. Noga and M. Magnuski, "High port-to-port isolation dual-polarized antenna array dedicated for full-duplex base stations," *IEEE Antennas Wireless Propag. Lett.*, vol. 19, no. 7, pp. 1098-1102, Jul. 2020.

[21] C. Ding, H. H. Sun, H. Zhu, and Y. J. Guo, "Achieving wider bandwidth with full-wavelength dipoles for 5G base stations," *IEEE Trans. Antennas Propag.*, vol. 68, no. 2, pp. 1119-1127, Feb. 2020.

[22] H.-H. Sun, H. Zhu, C. Ding, and Y. J. Guo, "Wideband planarized dual-linearly-polarized dipole antenna and its integration for dual-circularly-polarized radiation," *IEEE Antenna Wireless Propag. Lett.*, vol. 17, no. 12, pp. 2289-2293, Dec. 2018.

[23] C. Ding, H. Sun, R. W. Ziolkowski, and Y. J. Guo, "A dual layered loop array antenna for base stations with enhanced cross-polarization discrimination," *IEEE Trans. Antennas Propag.*, vol. 66, no. 12, pp. 6975-6985, Dec. 2018.

[24] H. Nawaz, N. Ahmad and J. Aslam, "A unidirectional, printed antenna with high interport isolation over wider bandwidth for 2.4 GHz full duplex applications," *IEEE Trans. Antennas Propag.*, vol. 69, no. 11, pp. 7183-7191, Nov. 2021.

[25] X. Yang, Y. Liu, Y. Xu and S. Gong, "Isolation enhancement in patch antenna array with fractal UC-EBG structure and cross slot," *IEEE Antennas Wireless Propag. Lett.*, vol. 16, pp. 2175-2178, 2017.

[26] N. -A. Nguyen et al., "Dual-polarized slot antenna for full-duplex systems with high isolation," *IEEE Trans. Antennas Propag.*, vol. 69, no. 11, pp. 7119-7124, Nov. 2021.

[27] Y. He and Y. Li, "Compact co-linearly polarized microstrip antenna with fence-strip resonator loading for in-band full-duplex systems," *IEEE Trans. Antennas Propag.*, vol. 69, no. 11, pp. 7125-7133, Nov. 2021.

[28] J. Hu, W. Zhang, Y. Li and Z. Zhang, "Compact co-polarized PIFAs for full-duplex application based on CM/DM cancellation theory," *IEEE Trans. Antennas Propag.*, vol. 69, no. 11, pp. 7103-7110, Nov. 2021

[29] Z. Wang, T. Liang and Y. Dong, "Compact in-band full fuplexing antenna for sub-6 GHz 5G applications," *IEEE Antennas Wireless Propag. Lett.*, vol. 20, no. 5, pp. 683-687, May 2021.

[30] M. E. Knox, "Single antenna full duplex communications using a common carrier," in *Proc. IEEE 13th Annu. Wireless Microw. Technol. Conf.*, Apr. 2012, pp. 1–6.

[31] E. A. Etellisi, M. A. Elmansouri, and D. S. Filipovic, "Wideband monostatic simultaneous transmit and receive (STAR) antenna," *IEEE Trans. Antennas Propag.*, vol. 64, no. 1, pp. 6–15, Jan. 2016.

[32] P. V. Prasannakumar, M. A. Elmansouri, and D. S. Filipovic, "Broadband reflector antenna with high isolation feed for full-duplex applications," *IEEE Trans. Antennas Propag.*, vol. 66, no. 5, pp. 2281–2290, May 2018.

[33] P. Valale Prasannakumar, M. A. Elmansouri, L. B. Boskovic, M. Ignatenko and D. S. Filipovic, "Wideband quasi-monostatic simultaneous transmit and receive reflector antenna," *IEEE Trans. Antennas Propag.*, vol. 68, no. 4, pp. 2630-2637, Apr. 2020.

[34] J. Ha, M. A. Elmansouri, P. Valale Prasannakumar and D. S. Filipovic, "Monostatic co-polarized full-duplex antenna with left- or right-hand circular polarization," *IEEE Trans. Antennas Propag.*, vol. 65, no. 10, pp. 5103-5111, Oct. 2017.

[35] A. H. Abdelrahman and D. S. Filipovi´c, "Antenna system for full-duplex operation of Handheld radios," *IEEE Trans. Antennas Propag.*, vol. 67, no. 1, pp. 522–530, Jan. 2019.
[36] E. A. Etellisi, M. A. Elmansouri and D. S. Filipović, "Wideband multimode monostatic spiral antenna STAR subsystem," *IEEE Trans. Antennas Propag.*, vol. 65, no. 4, pp. 1845-1854, Apr. 2017.
[37] M. Ranjbar Nikkhah, J. Wu, H. Luyen and N. Behdad, "A concurrently dual-polarized, simultaneous transmit and receive (STAR) antenna," *IEEE Trans. Antennas Propag.*, vol. 68, no. 8, pp. 5935-5944, Aug. 2020.
[38] M. A. Elmansouri, L. B. Boskovic and D. S. Filipovic, "Compact wideband dual-polarized in-band full-duplex antenna subsystem," *IEEE Trans. Antennas Propag.*, vol. 69, no. 11, pp. 7166-7172, Nov. 2021.
[39] K. Vaz and M. Caggiano, "Measurement technique for the extraction of differential s-parameters from single-ended s-parameters," in *Proc. 27th Int. Spring Seminar Electron. Technol.: Meeting Challenges Electron. Technol. Progress*, May 2004, vol. 2, pp. 313–317.
[40] H. Zhu, Z. Cheng, and Y. J. Guo, "Design of wideband in-phase and out-of-phase power dividers using microstrip-to-slotline transitions and slotline resonators," *IEEE Trans. Microw. Theory Techn.*, vol. 67, no. 4, pp. 1412–1424, Apr. 2019.
[41] H. Zhu, T. Zhang and Y. J. Guo, "Wideband hybrid couplers with unequal power division/arbitrary output phases and applications to miniaturized nolen matrices," *IEEE Trans. Microw. Theory Techn.*, early access.

Yue-Nian Chen (Student Member, IEEE) received the undergraduate degree in electronic and information engineering from Xidian University, Xi'an, China in 2018. He is currently enrolled in the five-year doctoral program in Xidian University and is also under the dual doctoral degrees program between Xidian University and University of Technology Sydney, Australia. His research interests include antenna decoupling, base station antennas and antenna technologies for 5G and 6G.

Can Ding (Member, IEEE) received the bachelor's degree in micro-electronics from Xidian University, Xi'an, China, in 2009, and the Ph.D. degree from Macquarie University, Sydney, Australia, in 2015. From 2012 to 2015, he was under the cotutelle agreement between Macquarie University and Xidian University. During that period, he was also with the Commonwealth Scientific and Industrial Research Organisation (CSIRO) DPaS Flagship, Marsfield, Australia. From 2015 to 2017, he was a Postdoctoral Research Fellow with the University of Technology Sydney (UTS), Sydney. He is currently a senior lecturer with the School of Electrical and Data Egineering (SEDE), the Faculty of Engineering and IT (FEIT) and he is also a core member of the Global Big Data Technologies Centre (GBDTC). He was awarded with Australian Research Council (ARC) Discovery Early Career Research Fellowship (DECRA) in 2020. His research interests include base station antennas, reconfigurable antennas, antenna decoupling and descattering, and advanced antenna technologies for 5G and 6G.

He Zhu (Member, IEEE) received the Bachelor's and Master's degree from South China University of Technology, Guangzhou, China, in 2011 and 2014, respectively, and the Ph.D. degree in Electrical Engineering from the School of ITEE, University of Queensland, Brisbane, Australia, in 2017. Since July of 2017, Dr. Zhu joined Global Big Data Technologies Centre (GBDTC), University of Technology Sydney (UTS), Ultimo, NSW, Australia, as a Post-doctoral Research Associate, where he is currently working as a Chancellor's Postdoctoral Research Fellow. Dr. Zhu received the Graduate School International Travel Award (GSITA) from the University of Queensland in 2015, the Dean's Award for Outstanding HDR Thesis from the University of Queensland in 2017. He is one of the recipients of the Chancellor's Research Fellowship from University of Technology Sydney in 2022. His research interests include development of passive and tunable microwave and mm-wave devices, radio frequency integrated circuits and systems, and beam-forming networks for antenna arrays.

Ying Liu (Senior Member, IEEE) received the M.S. and Ph.D. degrees in electromagnetics from Xidian University, Xi'an, China, in 2001 and 2004, respectively. From 2006 to 2007, she was a Post-Doctoral Research with Hanyang University, Seoul, South Korea. She is currently a Full Professor and the Lead of the National Key Laboratory of Science and Technology on Antennas and Microwaves, Xidian University. She has authored or coauthored over 200 refereed journal articles. She has also authored Prediction and Reduction of Antenna Radar Cross Section (Xi'an, China: Xidian Univ. Press, 2010) and Antennas for Mobile Communication Systems (Beijing, China: Electronics Industry Press, 2011). Her research interests include prediction and control of antenna radar cross section (RCS), and antenna theory and technology. Dr. Liu is a fellow of the Institution of Engineering and Technology (IET), the Chinese Institute of Electronics (CIE), and the China Institute of Communications (CIC). She is also the Chair of the IEEE AP Xi'an Chapter. She was a recipient of the "New Century Excellent Talents in University" of the Ministry of Education for China in 2011. She is also a reviewer for several international journals and serves as the TPC co-chair for several IEEE flagship conferences.